GASEOUS DETECTORS IN ASTROPHYSICS, MEDICINE AND BIOLOGY

FABIO SAULI

CERN, Geneva, Switzerland

ABSTRACT - Fast, position sensitive gaseous detectors have been developed mostly to satisfy the needs of elementary particle physics experimentation. We present some examples of use of those devices in other applied fields, from astrophysics to biology and medical research.

1. INTRODUCTION

Ionization chambers, proportional and Geiger counters have been in use for decades for detection of radiation. Large area, fast position-sensitive gaseous detectors based on the Multiwire Proportional Chamber (MWPC) [1] have been developed, primarily to satisfy the stringent demands encountered in particle experimental physics. Rather complex instruments, and therefore requiring dedicated operators, MWPCs and their offsprings represent in many cases unique tools for detection and localization of radiation; the continuing efforts to increase the ruggedness and reliability of the devices and the introduction of performing wireless detectors (parallel plate and microstrip gas chambers) permit to foresee an increasing use of gaseous detectors in other applied fields. This paper describes some examples of use of gaseous devices in medicine, biology and astrophysics.

2. APPLICATIONS OF MWPC

In a standard MWPC (see Fig. 1), electrons released by ionization in the gas are multiplied in the high electric field around thin wires. Various methods can be used to achieve localization: detection of pulses over threshold on anode wires, measurement of the center of gravity of signals induced by the avalanches on cathode strips, coupling of the signals to an external delay line, measurement of the collection or drift time of charges.
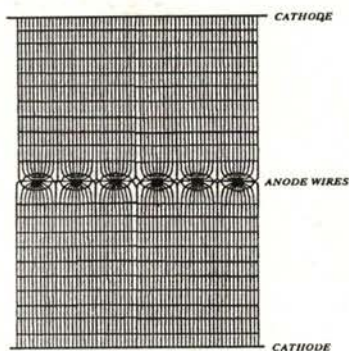
Fig. 1: Schematics of the Multiwire Proportional Chamber, showing the electric field lines and equipotentials.

Each method has advantages and drawbacks, and the choice is therefore application-specific.

In medicine and biology, a widely used readout method makes use of delay lines, that transform the space coordinate of the induced signals on cathodes into time delays, the signal detected on the anode wire plane being used to provide the reference time. The rate limitations and single hit capability of such readout method are compensated by the great simplicity and low cost.
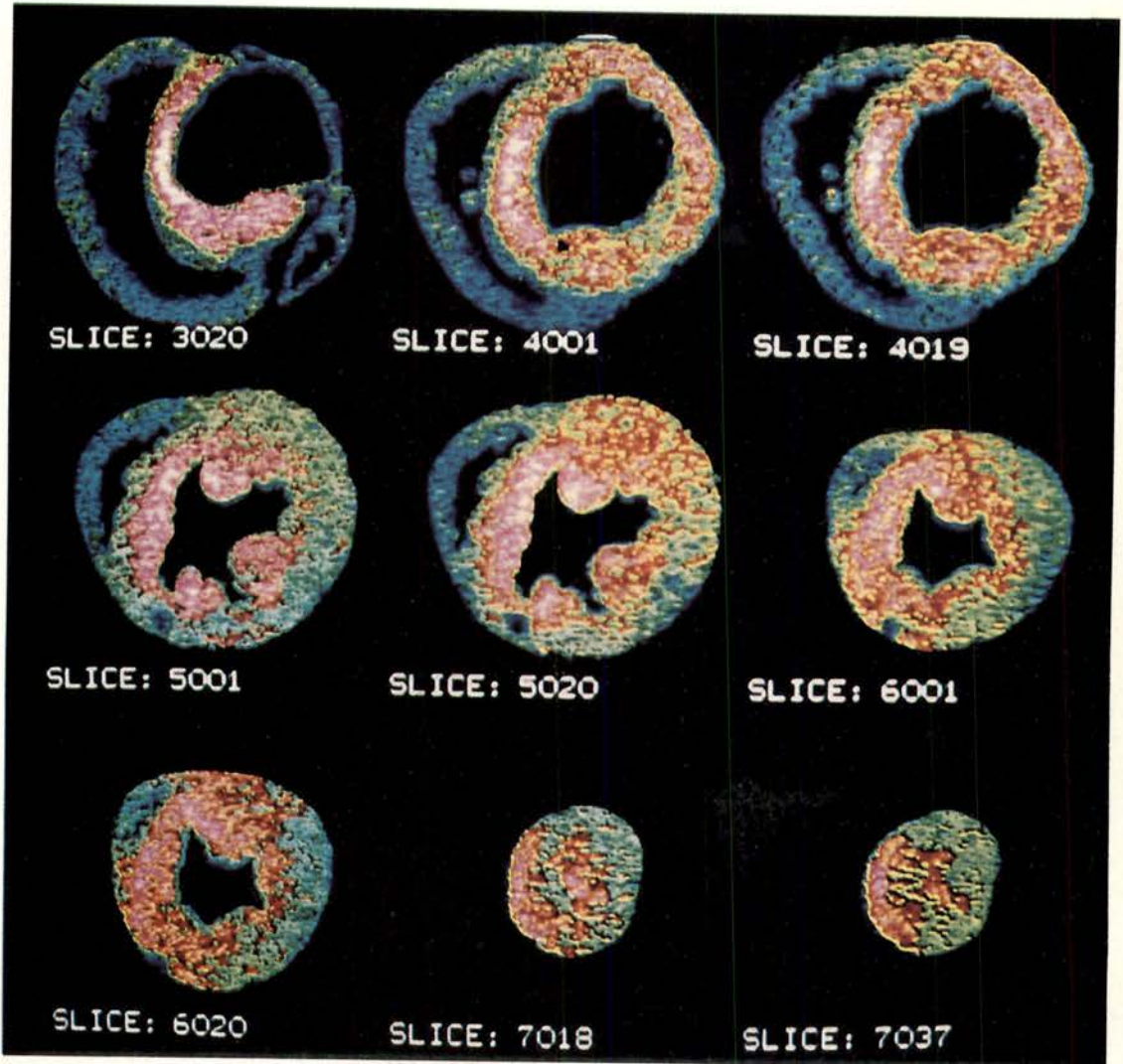
Fig. 2: Activity distribution in a slice of a dog's heart is recorded following repeated stimulation of specific cardio-pulmonary nerves after injection of triziated deoxyglucose.

Fig. 2 shows the beta activity distribution recorded with a MWPC with delay line readout in anatomical samples (slices of a dog's heart) labelled with tritiated deoxyglucose [2]. The experiment aims at studying the regional uptake of sugars in the heart under different stimulation conditions. Animals are open-chested after anesthesia, and selected efferent axons of cardiopulmonary nerves stimulated after injection of tritiated deoxyglucose. After excision, the distribution of the labeller is detected with the chamber and compared to normal distributions. Several hundred preparations can be analyzed in relative short times as compared to the use of photographic methods.
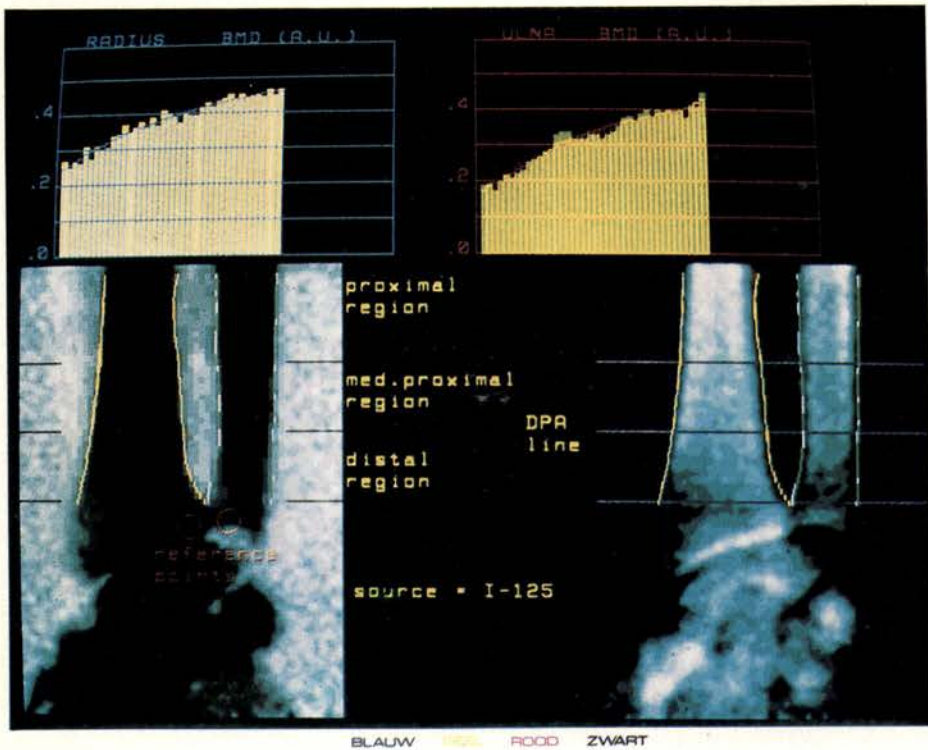
Fig. 3: Transmission radiography of limbs realized with a MWPC, showing examples of bone mineral content computed along selected directions.

With a similar apparatus, optimized for the detection of x rays in the range between 20 and 60 KeV, the same group has demonstrated the superior qualities of digital methods over photography in in the clinical measurement of bone mineral content in the peripheral skeleton [3]. A pressurized (3 bars) xenon-filled MWPC with delay line readout is used to detect and localize the photons at rates up to few hundred kHz. Single photon absorption (SPA) transmission

images are obtained using radioactive sources emitting photons at 27.4 KeV (^{125} I) and 42 KeV (^{153}Gd) (Fig. 3); the limb to be imaged is immersed in water, and the contribution of soft tissues can be subtracted making a transmission image of the bolus alone. In Double Photon Absorption (DPA), the soft tissue contribution is cancelled recording two images at different energies (27.4 KeV from ^{125} I and 60 KeV form ^{241}Am) and logarithmically subtracting the two after weighting.
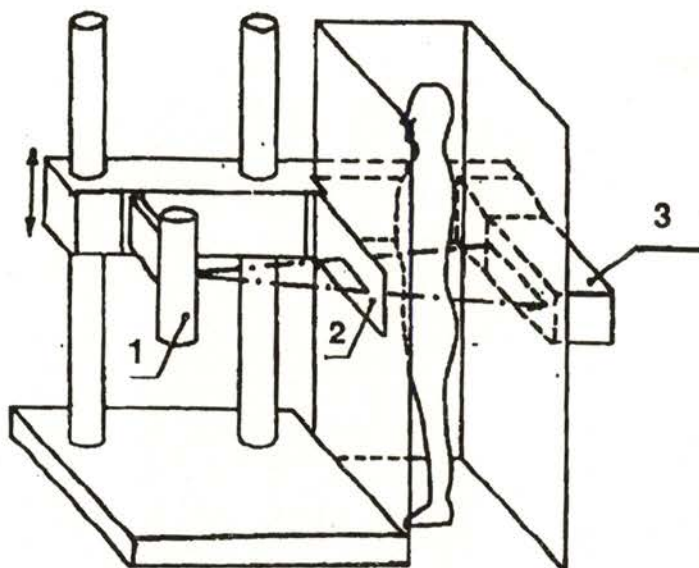
Fig. 4: Scanning system for transmission radiography using a high rate digital MWPC.

MWPC of conventional design are limited in their use to moderate acquisition rates, several hundred kHz or so over the whole detector, mostly because of the time necessary for transferring and recording the coordinate information. A simple counting of the hits on a wire can be done at much higher rates, but does not provide two-dimensional localization in conventional MWPC. A rather ingenious geometrical construction has been used to fully profit from the high intrinsic rate capability of the gas detectors for x-ray transmission radiography [4] (see Fig. 4).

The object is exposed to a beam of x rays emitted from a point source; the position detector, a pressurized xenon MWPC, is built with a particular geometry having non-parallel anode wires pointing to the source.
To compensate for the variable distance between anodes, affecting the gas gain, the anode to cathode distance is increased along the wires. All x-rays with the same angle are therefore detected by the same wire, and the counting rate on wires provides the absorption profile in the slice. Successive slices are obtained scanning through the body with the generator-detector system.

The system can acquire data at a rate in excess of 300 kHz per wire, with a position accuracy around 0.8 mm fwhm. Fig. 5 shows an example of transmission digital radiography of the chest obtained with the described apparatus in clinical conditions. The very low exposure dose (few mREM skin value) allows to foresee the use of the device in radiation-sensitive areas of the body.
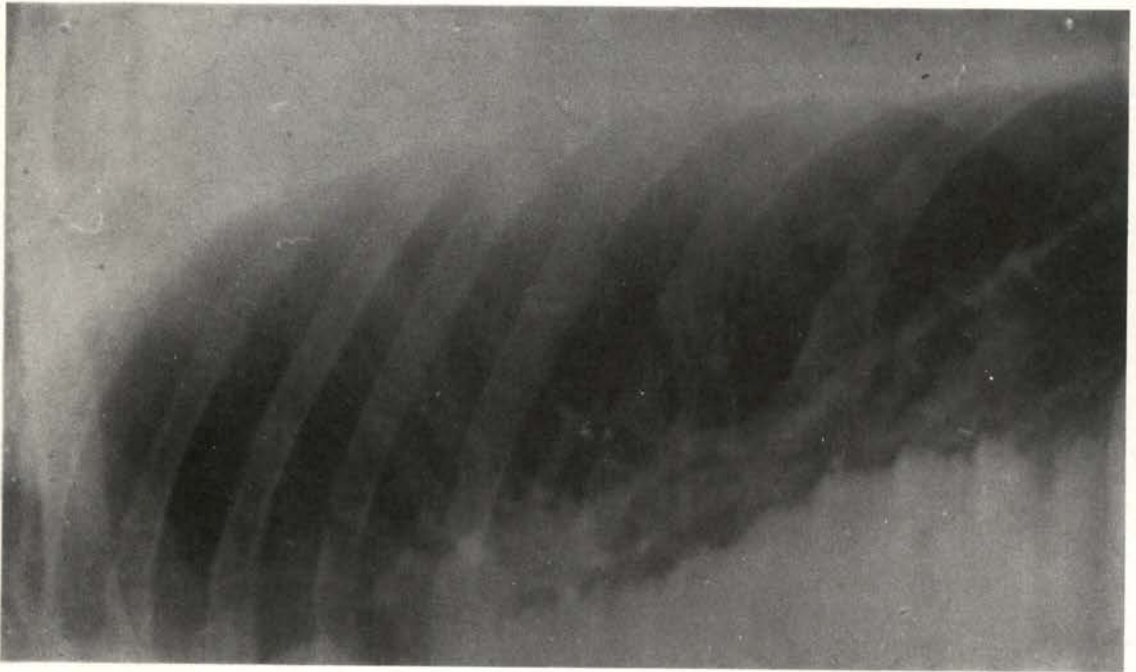
Fig. 5: Absorption radiography of the chest obtained with the high rate digital MWPC.

An example of direct use in astrophysics of technologies developed originally in high energy physics is given by the Cosmic Ray Tracking project, aimed at detection of extended air showers produced in the upper atmosphere by energetic photons [5]. The basic element of detection is shown in Fig. 6: it consists of a pair of large volume drift chambers separated by an iron plate-scintillator sandwich used for triggering and as muon filter. Tracking is realized measuring the drift time on anode wires and the induced signals on arrays of cathode pads in the central wire plane; muon identification is obtained by comparison of the tracks measured before and after the muon filter (electrons will either be absorbed or generate an electromagnetic shower).

Fig. 7 shows an example of cosmic shower detected recording the time profile of signals detected on six adjacent wires. The project foresees the installation of around 400 detector modules arranged in concentric rings and covering an area of about 3.10^5 square meters; thanks to the two-track resolu-tion of a few mm, as compared to centimeters in existing scintillation counters arrays, the detector improves sensitivity to extended air showers by two orders of magnitude in energy downwards, from 10^{14} to 10^{12} eV for the incoming photon.
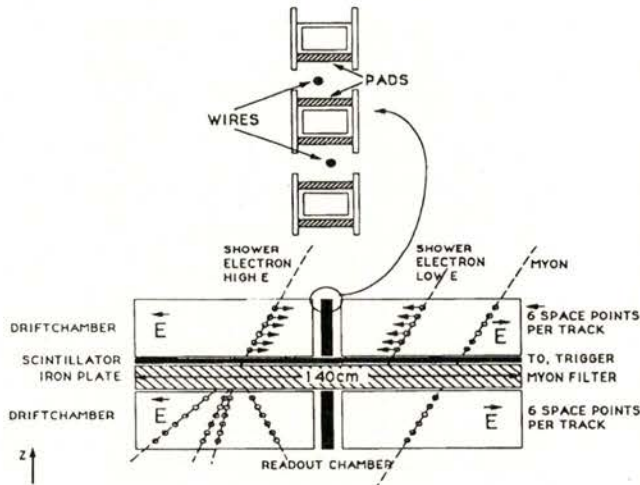
Fig. 6: Detector module for the cosmic ray tracking project. It consists of two independent chambers separated by a muon filter and scintillator.
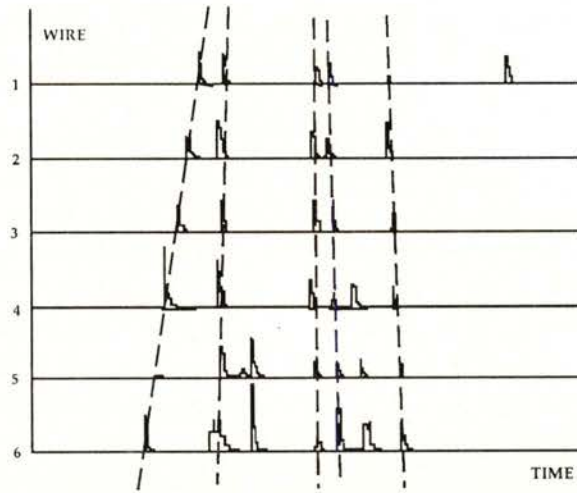
Fig. 7: A cosmic shower recorded by six drift wires equipped with flash analogue-to-digital converters.

3. THE IMAGING CHAMBER

Charge multiplication is exploited in gaseous counters for amplification of the ionization signal; photons are also copiously emitted in the avalanche as a result of molecular excitation and recombination processes. In imaging chambers, one detects and visualizes the emitted photons.
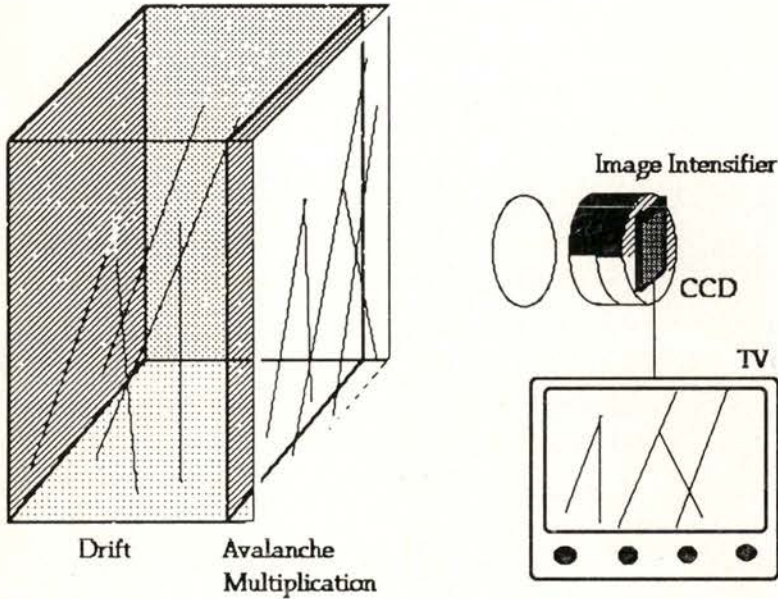
Fig. 8: Schematics of the imaging chamber. Electrons released in the gas volume drift to the parallel plate avalanche chamber. Photons emitted by the avalanches are detected by an image intensifier coupled to a solid state camera.

Addition of low ionization threshold vapors such as TEA[*] and TMAE[+] , together with the use of a parallel plate geometry (as against a MWPC structure), largely enhance the emission in a spectral region convenient for optical detection [6]. The structure of an Optical Imaging Chamber (OIC) is shown schematically in Fig. 8; electrons released in a gas by ionizing radiation drift under the influence of an electric field towards a region of very high field between two semi-transparent grids. During the avalanche development, photons are emitted and detected through a suitable window. An image intensifier is used to amplify the signal to a level compatible with the sensitivity of a solid state camera; the image can be

[*] TEA: Triethylamine, $(C_2H_5)_3N$
[+] TMAE: Tetrakis (dimethylamine) ethylene $[(CH_3)_2N]_2C = C[N(CH_3)_2]_2$

recorded directly or after digitization. To obtain high gains, one can use instead of a single amplification gap a multistep avalanche chamber ; to better tune the spectral emission to the sensitivity of the photon detector a thin foil wavelength shifter can be mounted in contact with the last electrode [7].

The simplicity and the high granularity of the device has suggested the application of the OIC in fields where these performances largely compensate for the modest data acquisition rate obtainable. An example is the visual detection in real time of cosmic rays is shown in Fig. 9. A device of this kind is operated at the Universal Exhibition in Sevilla to illustrate technological developments at CERN; a similar detector, installed at the CERN permanent exhibition "Microcosm", allows direct visualization of tracks produced by 5 MeV alpha particles.

Fig. 9: An example of cosmic activity recorded in a single frame with the video digitizer.

Use of the imaging chamber is being considered for an experiment aimed at detection of weakly interacting massive particles (WIMPs) [8]. The apparatus consists in a large volume of gas where recoil protons ejected off hydrogen or methane can be detected through amplification of the ionization trail in a geometry like the one shown in Fig. 8. To obtain measurable ranges for the low energy recoil protons (few KeV), the detector is operated at low pressures; in order to decrease the dispersing effect of diffusion on the drifting electrons, particularly large at low pressures, the device is operated in a strong magnetic field parallel to the drift direction. Simulations show that a distribution of

62

the end point of the recorded tracks, compensated for the daily rotation of earth, should be able to pinpoint galactic sources of the hypothetical WIMPs with a good degree of confidence. One can foresee the use of the imaging chamber in other astrophysics applications, for example in the detection of extended air showers generated by energetic gamma rays, described in the previous section.
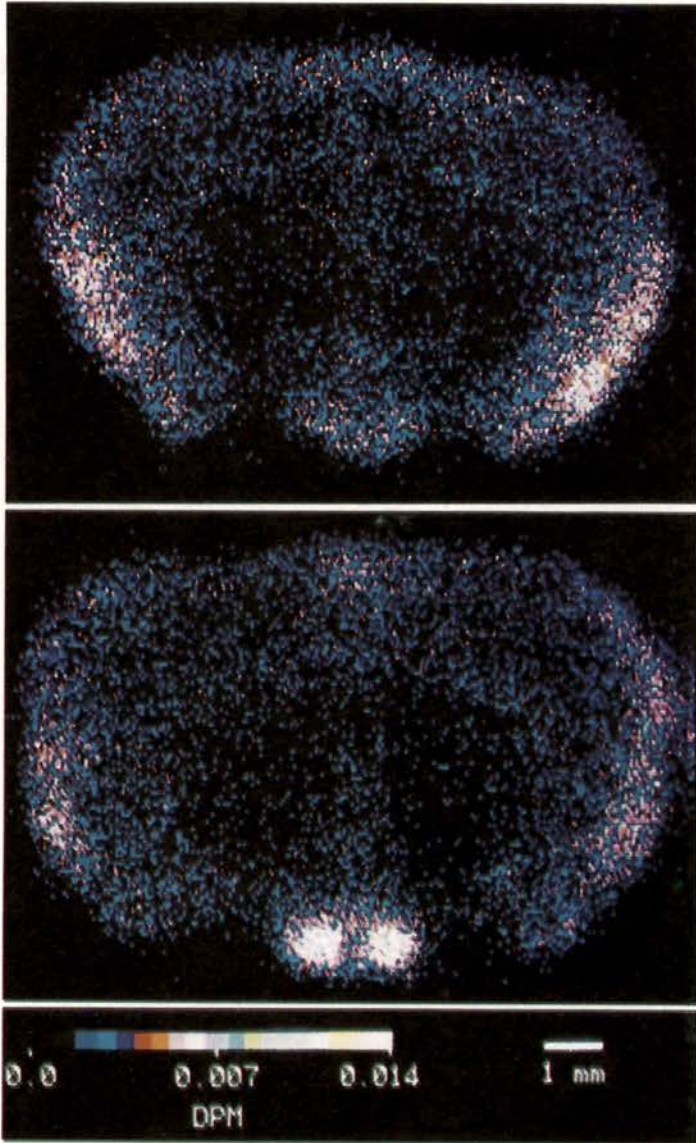
Fig. 10: Activity distribution in brain slices of male and female rats labelled with tritiated vasopressin (real size about 10 by 5 mm^2).

The OIC is being used in biology to map the two-dimensional activity distribution in anatomical samples marked with radioactive labellers [9]. Fig. 10 shows examples of activity distributions in anatomical samples (brain slices of male and female rats labelled with tritiated vasopressin*) recorded with the imaging chamber [10]; the study aims at establishing the effects of hormones release at the early stages of development on the sex of mature animals. Due to the sensitivity to individual radioactive decays, comparable contrasts are obtained with exposure times one or two order of magnitude shorter with the gaseous device as compared to film. This obviously allows the realization of exposure-intensive studies. Another advantage of the gas detector over conventional contact auto-radiography with is the linearity of the response over an extended range of activity, see Fig. 11 [10]; this allows quantitative analysis in a single exposure.

4. Microstrip Gas Chambers

This recently introduced gaseous detector [11] allows to overcome some restrictions met in classic multiwire structures, in particular the resolution and rate limitations resulting from the practical minimum wire pitch (a mm or so). As shown in Fig. 12, a Gas Microstrip Chamber (GMSC) consists in a set of thin parallel metal strips on an insulating substratum, alternately connected as anode and cathode; an upper electrode defines the sensitive volume of the chamber. Electrons released in the gas drift to the anode strips, where the high electric field induces avalanche multiplication as in a wire counter; a potential applied to the back plane prevents the collection of ions on the insulating substratum and minimizes gain-perturbing charging up processes.

The GMSC allows to reach gas gains around 10^4 with remarkably good energy resolutions (12% fwhm for the 5.9 keV x-rays [12]). The fast collection of most of the ions produced in the avalanche by the neighboring cathode strips imply also a very high rate capability, close to a MHz/mm^2 [13].

Several schemes can be used to readout the space coordinates of the detected radiation in the GMSC. A simple amplifier-discriminator on each anode strip will provide an accuracy corresponding to the pitch, while recording the profile of induced charge on cathode strips allows to get an accuracy of 30 µm rms for minimum ionizing particles [12]. A charge division readout method has been developed for the x-ray detector of the Soviet-Danish Röntgen Telescope, SODART , (Fig. 13 [14]). Groups of cathode strips are connected through a resistive chain, with readout amplifiers in discrete positions. The second coordinate is provided by a similar system mounted on an induction grid above the amplifying structure.

---

* AVP, [^{3}H] vasopressin

Although limited to moderate rates, the scheme allows to reduce the number of electronics channels to a minimum, a stringent requirement for space applications. Operating the detector with a xenon-CH4 mixture, the authors have demonstrated a position resolution around 340 µm rms for 5.9 keV x-rays; in two separate detectors optimized to cover the low and the high energy x-ray region respectively, the energy spectra shown in Fig. 14 a) and b) have been obtained.
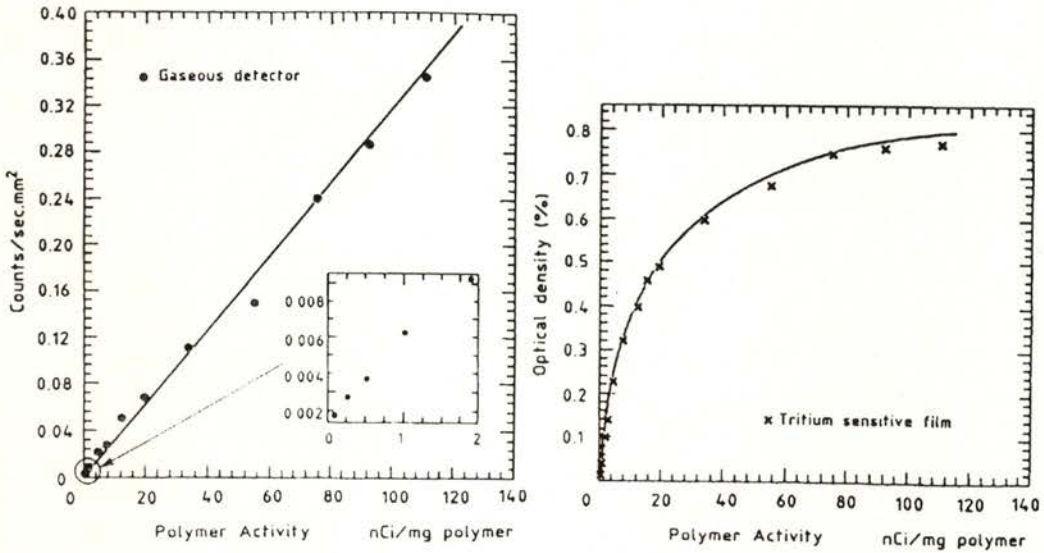
Fig. 11: Response of the imaging chamber (left) and of conventional film autoradiography to increasing activities of a tritiated polymer standard.
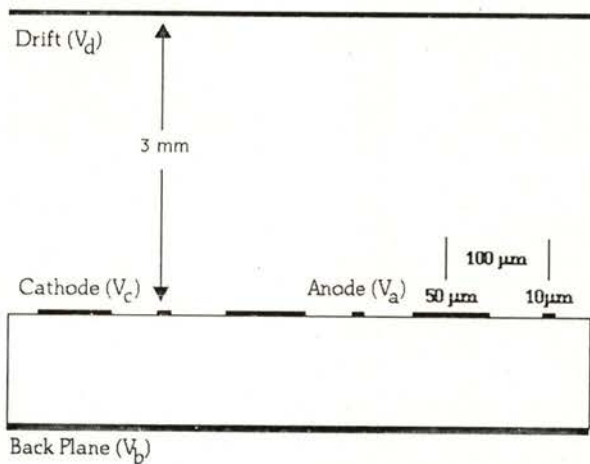
Fig. 12: Schematics of the microstrip gas chamber.

Use of the MSGC as detector for x-ray transmission radiography is also appealing because of the very high rate capability of the device. It has been recently demonstrated that MSGC can reliably operate in xenon mixtures at pressures up to 6 bars, a necessary requirement for obtaining efficient detection of x-rays at the energies used for clinical applications [15].
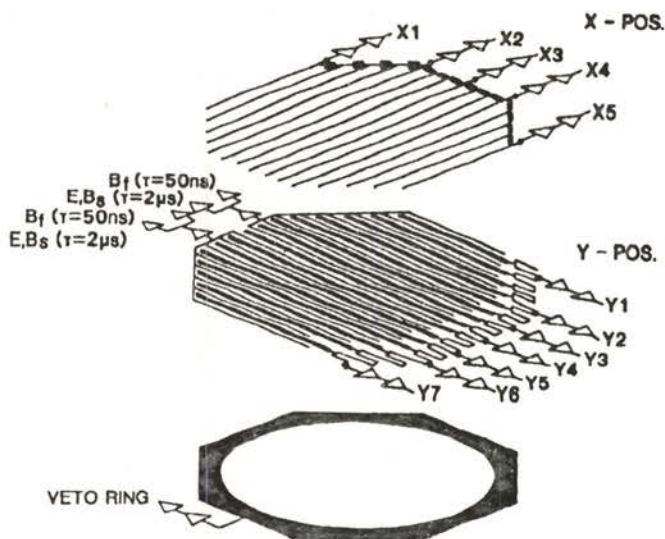
Fig. 13: Schematics of the charge division system foreseen for the readout of a MSGC used in the soviet-danish Röntgen telescope (SODART).
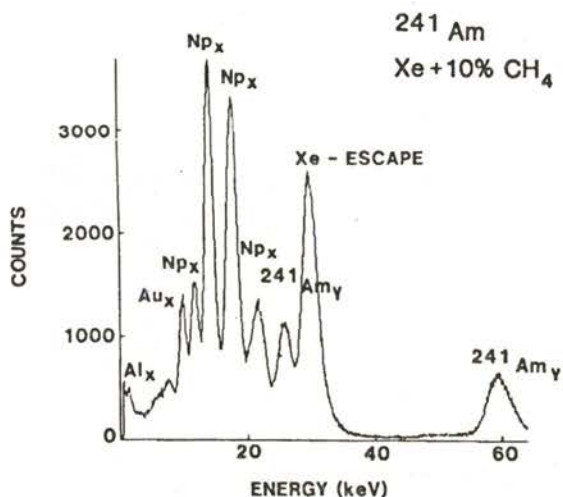
Fig. 14: Energy resolution of the MSGC built for SODART in the high energy x-ray region.

REFERENCES

[1] G. Charpak, Ann. Rev. Nuclear Sci. **20** 195 (1970).

[2] M. G. Trivella, J.A. Armour, M. Dalle Vacche, C. Paoli, R. Porinelli, R. Bellazzini, G. Pelosi, P. Camici, L. Taddei, G. A. Klassen and A. L'Abbate, Cardiovascular Research (1992).

[3] F. Angelini, R. Bellazzini, A. Brez, M.M. Massai, M. R. Torquati, G. Perri, D. Trippi, F. Beghé, Investigative Radiology **24** 684 (1989).

[4] S.E. Baru, A.G. Khabakhpashev, L.I. Shekhtman, Nucl. Instr. Methods **A283** 431 (1989).

[5] M. Feuerstack, J. Heinze, P. Lennert, B. Müller, S. Polenz, B. Cshmidt, J. Spizer, B. Stadler, S. Gamp, W. Hofmann, T. Kihm, J. Knöppler, M. Panter, B. Povh, C. Wiedner, Nucl. Instr. Methods **A310** 287 (1991).

[6] G. Charpak, J.-P. Fabre, F. Sauli, M. Suzuki and W. Dominik, Nucl. Instr. Methods **A258** 177 (1987).

[7] R. Bouclier, M. Bourdinaud, G. Charpak, P. Fonte, G. Million, F. Sauli and D. Sauvage, Nucl. Instr. Methods **A300** 286 (1991).

[8] K. Buckland, M. Lehner, G. Masek, M. Mojaver, Optical Readout of Prototype TPC WIMP Detector, Int. Rep. Univ. of California San Diego (Jan. 1992).

[9] W. Dominik, N. Zaganidis, P. Astier, G. Charpak, J.C. Santiard, F. Sauli, E. Tribollet, A. Geissbühler and D. Townsend, Nucl. Instr. Methods **A278** 779 (1989).

[10] E. Tribollet, J.J. Dreifuss, G. Charpak, W. Dominik and N. Zaganidis, Proc. Nat. Acad. Sci. USA **88** 1466 (1991).

[11] A. Oed, P. Convert, M. Berneron, H. Junk, C. Budtz-Jørgensen, M.M. Madsen, P. Jonasson, H.W. Schnopper, Nucl. Instr. Methods **A284** 223 (1989).

[12] F. Angelini, R. Bellazzini, A. Brez, M.M. Massai, G. Spandre, M. Torquati, R. Bouclier, J. Gaudaen and F. Sauli, Nucl. Phys. **23A** 254 (1991).

[13] R. Bouclier, J.J. Florent, J. Gaudaen, G. Million, A. Pasta, L. Ropelewski, F. Sauli and L.I. Shekhtman, Proc. Int. Vienna Wire Chamber Conf. 1992.

[14] C. Budtz-Jørgensen, A. Bahnsen, C. Olesen, M.M. Madsen, P. Jonasson, H.W. Schnopper, A. Oed, Nucl. Instr. Methods **A310** 82 (1991).

[15] F. Angelini, R. Bellazzini, A. Brez, M.M. Massai, L. Shekhtman, G. Spandre and M.R. Torquati, Proc. Int. Vienna Wire Chamber Conf.   1992.